Proceedings Paper:
Zaidi, SAR, McLernon, DC, Ghogho, M orcid.org/0000-0002-0055-7867 et al. (1 more author) (2015) Cloud Empowered Cognitive Inter-cell Interference Coordination for Small Cellular Networks. In: 2015 IEEE International Conference on Communication Workshop. 2015 IEEE International Conference on Communcation Workshop, 08-12 Jun 2015, London, UK. IEEE , pp. 2218-2224. ISBN 9781467363051

https://doi.org/10.1109/ICCW.2015.7247511

Cloud Empowered Cognitive Inter-cell Interference Coordination for Small Cellular Networks

Syed Ali Raza Zaidi, Desmond C. McLernon, Mounir Ghogho and Muhammad Ali Imran

***Abstract*—In this article, we present a Cloud empowered Cognitive Inter-Cell Interference Coordination (C^2-ICIC) scheme for small cellular networks. The scheme leverages a recently proposed cloud radio access network (C-RAN) architecture for enabling intra-tier coordination and relaxes the need for inter-tier coordination by adopting the phantom cell architecture. Employing tools from stochastic geometry, we characterize the downlink success probability for a Mobile User (MU) scheduled under the proposed coordination scheme. It is shown that, compared to un-coordinated scheduling, significant performance gains can be realized in ultra dense small cell deployment scenarios under the proposed C^2-ICIC scheme. This is attributed to the robust interference protection provisioned by the scheme. It is demonstrated that the gains are particularly large for the users experiencing a weak received signal strength. Indeed, for these users, the received signal-to-interference ratio (SIR) can only be improved by reducing the experienced aggregate co-channel interference. The closed-form expression derived for the downlink success probability is employed to quantify the link level throughput under the proposed scheme. Finally, we briefly explore the design space of the C^2-ICIC scheme in terms of interference protection cap which determines both the downlink throughput of the MU scheduled in the coordination mode and the transmission opportunity for the co-channel small cells.**

***Index Terms*—cloud cooperation, interference coordination, stochastic geometry, Poisson point process, cognitive interference, small cells**

I. Introduction

A. Motivation

NETWORK densification empowered by heterogeneous tiered small cell deployment is evolving as a promising solution to address the exponential hike in demand for high speed wireless connectivity. A recent report from Ericsson [1] predicts that around $5\times$ growth is expected in the number of mobile broadband consumers worldwide by 2017. Such a skyrocketing demand will be further complemented with the rapid proliferation of smart-phones, tablets, cyber-physical systems, internet-of-things (IoT)/machine-to-machine (M2M) communication devices and mobile cloud services. Consequently, it is predicted that while the voice traffic will maintain its current trend, the data traffic will grow 15 times by the end of 2017 [2]. Network densification using small cells is envisioned to be the key enabler for meeting such capacity demands. This has been recognized in 3GPP LTE release 10 and 12.

Aggressive frequency reuse combined with ultra-dense small cell deployment has been advocated by both academia and industry to improve the spectral efficiency by several orders of magnitude. However, the aggressive frequency reuse comes at a cost of increased co-channel interference. Consequently, the attainable performance of the network is mainly limited by the out-of cell interference. Realizing that interference is the main bottleneck, 3GPP LTE release 10 and 11 have proposed Enhanced Inter-Cell Interference Coordination (eICIC) schemes. In release 10, the concept of Almost Blank Sub-frame (ABS) was introduced to improve the downlink performance of a small cell user by scheduling it in the so called 'blank sub-frame' of the macro-cell. The concept was further extended to Reduced-Power Sub-frames (RPS) in LTE release 11 under the umbrella of Further enhanced Inter-Cell Interference Coordination (FeICIC). Interference coordination between the dominant interferers was also proposed in LTE release 10. Generally, the interference management techniques proposed under eICIC and FeICIC require either intra-tier and/or cross-tier coordination. With the traditional cellular architecture, such a coordination is attained by incurring significant additional overhead. The inter/intra-tier coordination is not only required for interference management but also plays a vital role in managing handovers for the mobile users.

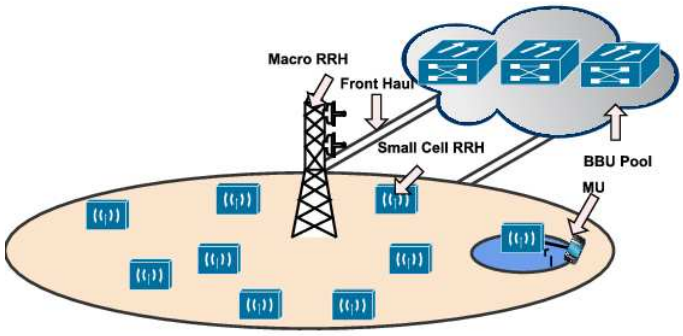

Figure 1: C^2-ICIC Network Architecture. For the sake of clarity, we do not show MU's associated with other small cell RRHs and the connection between each RRH and BBU pool using front haul.

Realizing that the coordination between cells is an essential ingredient of 5G cellular networks, China Mobile [3] has proposed an alternative cloud based architecture for small cell Remote Radio Head (RRH) deployment. The so called cloud empowered small-cellular networks leverages its flexible architecture to provide coverage and capacity expansion in a cost efficient manner. Unlike the conventional small cellular architecture, the cloud empowered network design exploits the advantage of centralized baseband processing to address the co-existence and scheduling issues. More precisely, the cloud small cell architecture decouples the Base-Band processing Unit (BBU) from the remote radio head. RRHs are connected to the cloud BBU pool via a flexible front-haul. The latter is usually an optical fiber where signaling is done using Radio-over-Fiber (RoF) or a Common Public Radio Interface (CPRI). Most of the baseband signal processing is delegated to the BBUs. In this article, we propose to empower the so called cognitive inter-cell interference coordination with cloud-based centralized cooperation.

B. C^2-ICIC Scheme

The inter-tier interference issue can be resolved by adopting the phantom small cellular architecture proposed by DOCOMO

S. A. R. Zaidi, D. C. McLernon and M. Ghogho are with the School of Electronic and Electrical Engineering, University of Leeds, United Kingdom; email: {s.a.zaidi, d.c.mclernon, m.ghogho}@leeds.ac.uk. M. Ghogho is also with the International University of Rabat. M. Imran is with the 5G Innovation Centre, University of Surrey, email: m.imran@surrey.ac.uk. This work is funded by USAITC-Atlantic under grant number W911NF-13-1-0216.

in [4], i.e., the small cells are deployed in a non co-channel mode. Specifically, the small and macro cells operate on different frequency bands. The architecture leverages a master-slave relationship between macro and small cells to provide a robust and scalable solution for rapid deployment of high throughput small cells. Small cells are delegated the responsibility of serving throughput intensive mobile users (MUs) while the macro-cell is responsible for handling the signaling and association. The architecture results in a control and capacity plane separation (frequently known as C/U plane split) providing support for adding on-demand capacity.

In order to address the intra-tier interference issue, i.e, the co-channel interference from other small cells, we consider a cognitive underlay inspired approach. Notice that the proposed approach is also inspired by the 3GPP proposed downlink high-interference indicator where a bitmap indicator, which is similar to the relative narrow-band transmit power (RNTP) indicator presented in Release 8, is employed for the identification of the dominant interferers. Furthermore, the proposed strategy is in principle similar to the cognitive underlay-based distributed interference protection (DIP) scheme which was introduced in [5]. The proposed scheme also resembles the dynamic frequency selection (DFS) specified in the 802.11h standard. To put the above mentioned architectural components in a unified framework, we propose a Cloud empowered Cognitive Inter-Cell Interference Coordination (C^2-ICIC) scheme whose operational details are summarized as follows:

1) Macro and small cells schedule their transmissions in different bands with central frequencies $f_{\mathcal{M}}$ and $f_{\mathcal{S}}$ and bandwidths $B_{\mathcal{M}}$ and $B_{\mathcal{S}}$, respectively. Due to the master-slave relationship between the macro and small cells, a macro cell can also broadcast control signals/pilots in the small cells transmission band.
2) A MU is assigned to a certain small cell based on some association criterion. In order to initiate the process of intra-tier interference coordination, the serving cell broadcasts a pilot sequence which is correlated with the known pilot template at the MU. The MU then re-broadcasts the received pilot signal.
3) The co-channel small cells listen to the broadcast of the pilot from the scheduled MU terminal. The received pilot is employed to estimate the channel between the small cells and the scheduled MU. Each co-channel small cell then estimate the channel gain and compares it to a pre-defined interference threshold. If the channel gain is below a certain threshold, the small cell can schedule its corresponding users in the current sub-frame; otherwise, the transmissions are deferred in order to control interference. The pre-defined interference threshold is designed adaptively in the cloud. The threshold adaptation is required to cater for the variation in density of the MUs over the temporal dimension which in turn impacts the number of active serving RRHs. Fig. 1 provides a graphical illustration of the overall architecture.

In this article, we focus our attention towards characterizing the downlink performance of a scheduled MU under the proposed C^2-ICIC scheme. We demonstrate that the interference threshold selection has to be carefully investigated in order to optimize the network area spectral efficiency[1]. However, such optimization is not addressed in this paper due to space limitation.

[1]Note that only the few MUs whose QoS requirements are not met using the non-coordination mode will be scheduled under the coordination mode, though not simultaneously. The other MUs are served normally by their cells without requiring any coordination with other cells.

Assumption 1: It is assumed that the C^2-ICIC scheme is employed in a certain sub-frame to enhance the performance of a MU whose QoS cannot be fulfilled otherwise. Hence, *only one* MU can be scheduled in the proposed coordination mode in each sub-frame per macro-cell. While a designated RRH serves this MU, the proposed interference coordination strategy will dictate which of the other RRHs may serve their corresponding MUs in the non-coordination mode.
A trivial way of controlling interference would be to turn off all other RRHs during the coordination sub-frame. This would however result in the implementation of an intra-tier ABS which incurs a significant penalty in terms of network level throughput.

C. Contributions

Developing an accurate analytical model for the aggregate co-channel interference under the C^2-ICIC scheme plays a central role towards characterizing the attainable performance for a scheduled MU. In this paper, we use stochastic geometry to model the spatial distribution of the small cells, and use the downlink throughput as a key metric towards investigating the attainable link level performance. The downlink throughput is defined as the product of the attainable rate for a certain desired signal-to-interference-plus-noise-ratio (SINR) threshold (obtained by employing the Shannon formula) and the success probability for the desired SINR threshold. The co-channel interference has a similar structure as in [5] [6] and [7]. However, inspired by the interference modeling in the context of CRs (see for e.g. [5], [8], [9], [10], [11], [12]), the authors of these papers also rely on the moment matching approach to compute the *approximate* PDF of the aggregate interference. Consequently, the analysis inherits the following limitations:

- The aggregate *interference distribution* and not the *distribution of* SIR was characterized. The success probability (SP) of the downlink between the MU and the serving cell is a more meaningful performance metric than the probability of experiencing a certain level of interference, from a network designer perspective. Further, analysis based on the approximate distribution in [5] is intricate if not impossible. The widely utilized distributions such as the *shifted Log-normal* or *Log-normal* distribution do not possess a closed form expression for their Laplace transform/characteristic function. Hence, the characterization of the SP is difficult even when the communication channel suffers from *Rayleigh flat fading* (see Section III for the relation between SP and the Laplace transform).
- Since the existing approaches rely on *approximation*s, the analysis based on the corresponding distributions *cannot provide* any performance *guarantees*. Most of these approximations are only valid for a limited choice of parameters. Moreover, for instance in [6] and [7], it can be noticed that such approximations are quite poor towards the tail of the distribution. It is precisely the tail regime which plays a central part in the characterization of the attainable performance.

To the best of the authors' knowledge, the exact characterization of the aggregate interference and thus the attainable performance under the proposed coordination strategy has not been addressed before. Notice that such a characterization is important for exploring the design space for the optimization of the network level performance. In this article, our objective is to provide an exact analytical quantification of the performance obtained under the proposed C^2-ICIC scheme. Contrary to the existing literature, our performance evaluation also accounts for more realistic propagation conditions by considering the composite shadow-fading channel (see Section II).

Cloud coordinated small cells have recently received a significant attention from academia and industry. A detailed survey of the coordination schemes, which have been proposed to either reduce the load on front haul by signal compression [13] or to improve the performance of MUs by joint transmission [14], is beyond the scope of this article. Relevant discussions can be found in [13] and [14].

D. Organization

The network model, spatial topology and propagation characteristics are described in Section II. In order to characterize the spectral efficiency of the link between the MU and the serving small BS, we derive a closed-form expression for the SP in Section III. These results are validated via extensive Monte-Carlo simulations. Also in Section III, the formal definition and quantification of the spectral efficiency is pursued. Finally, conclusion are presented in Section IV.

E. Notations

Throughout the paper, we use bold-face small letters (e.g. $\boldsymbol{x}$) to denote the location of the node and to refer to the node itself. Statistical expectation is denoted by $\mathbb{E}(.)$. In order to simplify the notations, both a random variable and its corresponding realization are denoted by the same lower case letter, e.g., h. The probability of event A is denoted as $\mathbb{P}(A)$. Finally, $h \sim \mathcal{N}(\mu, \sigma^2)$ means that random variable h has a standard normal distribution with mean μ and variance σ^2.

II. Network and Channel Model

A. Spatial Model for Small Cell RRHs

We consider a typical small cell (say $\boldsymbol{x}$) located at a distance r_l from the MU (say $\boldsymbol{o}$) it intends to serve. For the sake of analytical tractability, we assume that $\boldsymbol{o}$ is located at the origin. The spatial distribution of the other small cell RRHs is captured using a *homogenous Poisson point process* (HPPP) [15] $\Pi_{\mathcal{S}}^{TX}$ with intensity $\lambda_{\mathcal{S}}$ on $\mathbb{R}^2$. Here, $\lambda_{\mathcal{S}}$ is the average number of RRHs per unit area. More specifically, the probability of finding $n \in \mathbb{N}$ nodes inside a region $\mathcal{A} \subseteq \mathbb{R}^2$ follows a Poisson law with the mean measure $\Lambda(\mathcal{A}) = \lambda_{\mathcal{S}} \int_{\mathcal{A}} dx$ [15].

Assumption 2: It is assumed that $\boldsymbol{x} \notin \Pi_{\mathcal{S}}^{TX}$.
Although the above assumption simplifies the analytical analysis, the presented analysis can be easily extended to a more general case where $\boldsymbol{x} \in \Pi_{\mathcal{S}}^{TX}$. In this case, $\boldsymbol{x}$ may be chosen to be the nearest neighbor to $\boldsymbol{o}$, i.e. $\boldsymbol{o} \in \mathcal{C}_{\boldsymbol{x}}$ where $\mathcal{C}_{\boldsymbol{x}} = \left\{\boldsymbol{z} \in \mathbb{R}^2 : \|\boldsymbol{x}-\boldsymbol{z}\| \leq \|\boldsymbol{x}-\boldsymbol{y}\|, \boldsymbol{y} \in \Pi_{\mathcal{S}}^{TX} \backslash \{\boldsymbol{x}\}\right\}$is the Voronoi cell of $\boldsymbol{x}$. In this case, r_l is a random variable with Rayleigh distribution. Also, this results in an exclusion zone for $\boldsymbol{y}$ given by a disc or radius r_l centered on $\boldsymbol{o}$. Our analysis can be easily extended to this case by averaging the MU SP with respect to the distribution of r_l and changing the lower limit of the integrals in (9) & (13) to r_l. However, in this paper, we do not consider such generalization of our results using the Voronoi based association approach to keep the analysis simple and thus obtain useful design insights.

B. Channel Model

We assume that both types of links, i.e., the link from the serving small cell RRH to its intended MU ($\boldsymbol{x} \rightarrow \boldsymbol{o}$) and the other cell interference links ($\boldsymbol{y} \rightarrow \boldsymbol{o}, \forall \boldsymbol{y} \in \Pi_{\mathcal{S}}^{TX}$) experience a composite Lognormal-Nakagami shadow-fading channel. The overall channel gain between a transmitter and a receiver separated by a distance r is thus modeled as $hl(r)$. Here, $h = g_1 g_2$ with g_1 capturing the impact of the large-scale shadowing and g_2 capturing the small-scale flat fading, i.e.,

- g_1 follows the Log-normal distribution which can be represented as $g_1 = \exp(\zeta \sigma z)$ where $z \sim \mathcal{N}(0,1)$ and $\zeta = {\ln(10)}/{10}$. The parameter σ captures the severity of the shadowing experienced by the link. We denote the fading severities of the communication and interference links by $\sigma_{\boldsymbol{ox}}$ and $\sigma_{\boldsymbol{oy}}$, respectively.
- g_2 follows the Gamma distribution with shape parameter $k = m$ and scale parameter $\theta = \frac{1}{m}$. The parameter m captures the fading severity of the propagation channel. The severity decreases with an increasing value of m. We consider that the desired communication link experiences a Nakagami channel with fading severity $m_{\boldsymbol{ox}}$, while the fading severity of the interference link is denoted by parameter $m_{\boldsymbol{oy}}$. We assume that both $m_{\boldsymbol{ox}}$ and $m_{\boldsymbol{oy}}$ assume integer values.

The large-scale path-loss is modeled by $l(r) = Kr^{-\alpha}$, which depends on the distance r, a frequency dependent constant K and an environment/terrain dependent path-loss exponent $\alpha \geq 2$. The fading channel gains are assumed to be mutually independent and identically distributed (i.i.d.). Without loss of generality, we will assume $K = 1$ for the rest of this discussion. It is assumed that the link between a MU and the serving small cell RRH is interference limited and hence the thermal noise is ignored in our analysis. It is assumed that the small cell RRHs transmit with a fixed transmission power $P_s \leq P_{max}$where P_{max} is the maximum allowable transmit power set by the spectrum regulatory body. Note that the proposed analysis can be extended for transmit power adaptation schemes in a straight-forward manner. Notice that our main interest lies in quantifying the SP of the scheduled MU under worst case propagation conditions, i.e. Rayleigh fading with Log-normal shadowing. However, we consider Nakagami fading model to demonstrate the generality of the proposed modeling framework.

C. Co-existence Strategy Model

As described in Section I-B, the C^2-ICIC scheme can be modeled as a medium access scheme enforced on the co-channel small cell RRHs which intend to serve their own users concurrently. In other words, the C^2-ICIC scheme limits the interference experienced at an MU scheduled in the coordination mode by silencing the co-channel RRHs for which the following interference indicator is zero:

$$\mathbb{1}_{I_{th}}(r_{\boldsymbol{y}}, h_{\boldsymbol{y}}) = \begin{cases} 1, & \Omega(r_{\boldsymbol{y}}, h_{\boldsymbol{y}}) \leq I_{th} \\ 0, & \text{otherwise} \end{cases}. \tag{1}$$

for $\boldsymbol{y} \in \Pi_{\mathcal{S}}^{TX}$, where $\Omega(r_{\boldsymbol{y}}, h_{\boldsymbol{y}}) = P_s h_{\boldsymbol{y}} l(r_{\boldsymbol{y}})$ with $r_{\boldsymbol{y}} = \|\boldsymbol{y} - \boldsymbol{o}\| = \|\boldsymbol{y}\|$ being the distance between the co-channel small cell RRH $\boldsymbol{y}$ and the MU, $\boldsymbol{o}$, located at the origin, and h_y captures the interference channel gain. Notice that in the presence of shadow-fading, the C^2-ICIC scheme results in a soft-exclusion rule for the co-channel transmitters.

III. Performance Analysis of C^2-ICIC

The main objective of this section is to quantify the performance gain obtained under the proposed C^2-ICIC scheme. To that end, we first quantify the link SP of the MU scheduled with and without the coordination mode. The derived closed-form expression for the downlink SP is then used to quantify the link level throughput. The downlink SP can be mathematically defined as $\mathbb{P}_{\mathcal{MU}}(\gamma_{th}, r_l) = \Pr\{\Gamma_{\mathcal{MU}} \geq \gamma_{th}\}$, where $\Gamma_{\mathcal{MU}} = {P_s h_{\boldsymbol{x}} l(r_l)}/{I_s}$ is the downlink SIR in the presence of aggregate co-channel interference I_s.

In order to quantify the downlink SP, we first present a general Lemma to establish the relationship between the Laplace transform of the aggregate interference and the downlink SP.

Lemma 1 (Relationship between the SP and the Laplace transform of the aggregate interference)**.** *Consider a downlink for a MU ($\boldsymbol{o}$) scheduled in the presence of co-channel small cell RRHs which can be modeled by a Poisson process*[2] $\Pi \subseteq \Pi_{\mathcal{S}}^{TX}$*. Under the composite Nakagami-Log normal fading, the link SP can be quantified in terms of the Laplace transform of the aggregate co-channel interference as follows*

$$\mathbb{P}_{\mathcal{MU}}\left(\gamma_{th}, r_l\right) = \sum_{i=0}^{m_{\boldsymbol{ox}}-1} \frac{(-s)^i}{i!} \frac{\partial^i \mathcal{L}_I(s)}{\partial s^i}\bigg|_{s=\gamma_{th} r_l^{\alpha}}, \tag{2}$$

where $I = \sum_{\boldsymbol{y}\in\Pi} h_{\boldsymbol{y}} l(r_{\boldsymbol{y}})$ is the aggregate interference and $\mathcal{L}_I(s) = \mathbb{E}_I(\exp(-sI))$ is the Laplace transform of the aggregate interference .

Proof. See Appendix A. □

A. Downlink SP without C^2-ICIC

To obtain a better understanding of the performance gains experienced under the proposed coordination scheme and the price paid for such gains, we first quantify the performance for a MU scheduled in the absence of such scheme.

Theorem 1 (SP without C^2-ICIC)**.** *The downlink SP for a MU $\boldsymbol{o}$ served by the small cell RRH located at distance r_l can, under the composite Nakagami-Lognormal fading, be quantified as in Eq. (3) with $\delta = \frac{2}{\alpha}$.*

Proof. See Appendix B. □

Remarks

1) An increase in $m_{\boldsymbol{ox}}$ corresponds to a decrease in the fading severity. Consequently, with an increase in $m_{\boldsymbol{ox}}$ the link SP increases; indeed, increasing m will result in more positive terms in the summation of (3)[3]. Similarly, it is easy to observe that the downlink SP decays exponentially with an increase in the shadowing severity.
2) The downlink SP is a function of the link distance and thus a MU which lies far from the serving small cell RRH has worst performance as compared to a MU which lies close to RRH. Note that the link SP is also a function of the product of the density of the co-channel interferers and the link distance (for instance in the case of Rayleigh fading $\log\left(\mathbb{P}_{\mathcal{MU}}^{wo}\right) = -\kappa_1 \gamma_{th}^{\delta} r_l^2 \lambda_{\mathcal{S}}$); this implies that to keep the same SP, in the coordination mode, the cell density must be decreased (through silencing) proportionally to the squared growth in the link distance.

B. Downlink SP under C^2-ICIC

It can be easily shown that the gain experienced in terms of link SP improvement under the proposed C^2-ICIC can be quantified as

$$\eta = \left| \frac{\mathbb{P}_{\mathcal{MU}}^{w}\left(\gamma_{th}, r_l\right) - \mathbb{P}_{\mathcal{MU}}^{wo}\left(\gamma_{th}, r_l\right)}{\mathbb{P}_{\mathcal{MU}}^{wo}\left(\gamma_{th}, r_l\right)} \right| \times 100\%, \tag{5}$$

where $\mathbb{P}_{\mathcal{MU}}^{w}\left(\gamma_{th}, r_l\right)$ is the link SP when the MU is scheduled under the coordination mode. The quantification of $\mathbb{P}_{\mathcal{MU}}^{w}\left(\gamma_{th}, r_l\right)$ is pursued in this sub-section.

[2]Not necessarily *homogenous* Poisson process.

[3]Notice that the negative sign of s is counteracted by the negative sign in the exponential due to derivatives.

Theorem 2 (SP with the C^2-ICIC scheme)**.** *The SP of the link between a MU ($\boldsymbol{o}$) and its intended serving small cell RRH ($\boldsymbol{x}$) in the presence of the co-channel small cell RRHs operating under the C^2-ICIC scheme can be quantified using Eq. (4).*

Proof. In order to exploit Lemma 1 to quantify the downlink SP, the Laplace transform of the aggregate interference generated under the C^2-ICIC scheme must be quantified. The aggregate interference at the MU is given as

$$I = \sum_{\boldsymbol{y}\in\Pi_{\mathcal{S}}^{TX}} h_{\boldsymbol{y}} l(r_{\boldsymbol{y}}) \mathbb{1}_{I_{th}}(r_{\boldsymbol{y}}, h_{\boldsymbol{y}}). \tag{6}$$

where I is the co-channel interference generated by a Marked Poisson point process (MPPP) $\bar{\Pi}_{\mathcal{S}}^{TX}$ on $\mathbb{R}^2 \times \mathbb{R}^+$, constructed from the HPPP $\Pi_{\mathcal{S}}^{TX}$ by pairing i.i.d. marks for the fading channel gain between the co-channel RRHs and $\boldsymbol{o}$ to each concurrent transmitter, i.e., $\bar{\Pi}_{\mathcal{S}}^{TX} = \{[\boldsymbol{y}; h_{\boldsymbol{y}}] : \forall \boldsymbol{y} \in \Pi_{\mathcal{S}}^{TX}\}$. Under the C^2-ICIC in (1), the active co-channel RRHs form a non-homogenous Poisson point process Π_I on $\mathbb{R}^2 \times \mathbb{R}^+$ constructed by the thinning [15] of $\bar{\Pi}_{\mathcal{S}}^{TX}$ given by

$$\Pi_I = \{[\boldsymbol{y}; h_{\boldsymbol{y}}] \in \bar{\Pi}_{\mathcal{S}}^{TX} : \mathbb{1}_{I_{th}}(r_{\boldsymbol{y}}, h_{\boldsymbol{y}}) = 1\}. \tag{7}$$

Employing the mapping theorem in [15], the point process can be easily transformed to polar coordinates. So the intensity function of the point process Π_I is given by

$$\lambda_I(r, h) = \lambda_{\mathcal{S}}^{TX} 2\pi r \mathbb{1}_{I_{th}}(r, h)\, f_H(h) \tag{8}$$

where, $f_H(h)$ is the PDF of the modified composite shadow-fading random variable H. Now the Laplace transform of the aggregate interference I can be evaluated using the definition of the Generating functional for the Marked Poisson point process [15] as

$$\mathcal{L}_I(s) = \exp\left(- \underbrace{\int_0^{\infty}\int_0^{\infty} \left(1 - \exp\left(-shr^{-\alpha}\right)\right) \lambda_I(h,r)\, dr\, dh}_{A_1} \right) \tag{9}$$

Detailed derivations are provided in Appendix C. □

From Eq. (4) it can be easily observed that:

1) $\lim_{I_{th}\to\infty} \mathbb{P}_{\mathcal{MU}}^{w}\left(\gamma_{th}, r_l\right) \rightarrow \mathbb{P}_{\mathcal{MU}}^{wo}\left(\gamma_{th}, r_l\right)$ since $\lim_{I_{th}\to\infty} \gamma_l(1-\delta, s\bar{I}_{th}) \rightarrow \Gamma(1-\delta)$. In other words, for a very high interference tolerance threshold, as expected, the link SP performance of the C^2-ICIC scheme converges to the case where no coordination is implemented.
2) $\lim_{I_{th}\to 0} \mathbb{P}_{\mathcal{MU}}^{w}\left(\gamma_{th}, r_l\right) \rightarrow 1$, i.e. for a very stringent zero interference tolerance, the link SP naturally tends to unity.

C. Discussion & Validation

The derived analytical results for quantifying the downlink SP are corroborated through Monte-Carlo simulations. Fig. 2 depicts the downlink SP of the scheduled MU under the proposed interference coordination scheme as a function of its desired SIR threshold for various propagation conditions and active co-channel small cell RRH densities. The Monte-Carlo simulations used 10^4 realizations for both Π_s^{TX} and the fading-channel gains, for each SIR threshold (γ_{th}). As is clear from Fig. 2 the theoretical results obtained using Eq. (4) are indistinguishable from the simulation results.

Fig. 2 indicates that the SP of the scheduled MU decreases with an increase in fading severity of the communication channel (i.e., $m_{\boldsymbol{ox}}$). As expected the worst case performance is experienced

$$\mathbb{P}^{wo}_{\mathcal{MU}}\left(\gamma_{th}, r_l\right) = \sum_{i=0}^{m_{\boldsymbol{ox}}-1} \frac{(-s)^i}{i!} \frac{\partial^i}{\partial s^i} \exp\left(-\lambda_{\mathcal{S}} \underbrace{\pi \frac{\Gamma\left(m_{\boldsymbol{oy}}+\delta\right)\Gamma\left(1-\delta\right)}{\Gamma\left(m_{\boldsymbol{oy}}\right) m_{\boldsymbol{oy}}^{\delta}} \exp\left(\frac{\mu^2}{2}\right)}_{\kappa_1} s^{\delta} \right) \Bigg|_{s=\gamma_{th} r_l^{\alpha}}, \tag{3}$$

where $\mu = \delta\left(\sigma_{\boldsymbol{ox}} + \sigma_{\boldsymbol{oy}}\right)\zeta$ and $\Gamma(a) = \int_0^{\infty} x^{a-1}\exp(-x)dx$.

$$\mathbb{P}^{w}_{\mathcal{MU}}\left(\gamma_{th}, r_l\right) = \sum_{i=0}^{m_{\boldsymbol{ox}}-1} \frac{(-s)^i}{i!} \frac{\partial^i}{\partial s^i} \exp\left(\frac{-\lambda_{\mathcal{S}}\pi\Gamma\left(m_{\boldsymbol{oy}}+\delta\right)\left\{s^{\delta}\gamma_l\left(1-\delta, s\bar{I}_{th}\right) - \bar{I}_{th}^{-\delta}\left(1-\exp\left(-s\bar{I}_{th}\right)\right)\right\}}{\Gamma(m_{\boldsymbol{oy}}) m_{\boldsymbol{oy}}^{\delta}} \exp\left(\frac{\mu^2}{2}\right) \right) \Bigg|_{s=\gamma_{th} r_l^{\alpha}}, \tag{4}$$

where $\gamma_l(a,b) = \int_0^b t^{a-1}\exp(-t)dt$ and $\bar{I}_{th} = {}^{I_{th}}/_{P_s}$.

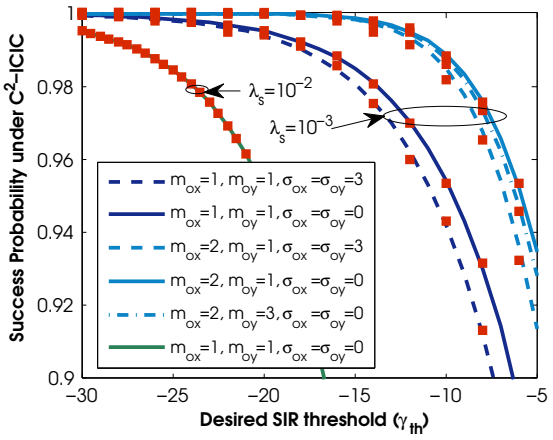

Figure 2: Downlink SP for a MU under the C^2-ICIC with a varying desired SIR threshold (γ_{th}) when $\alpha = 4$, $I_{th} = -5$ dBm, $r_l = 10$ and $P_s = 1$. Solid and dashed lines are obtained via (4) while '■' represents Monte-Carlo simulations.

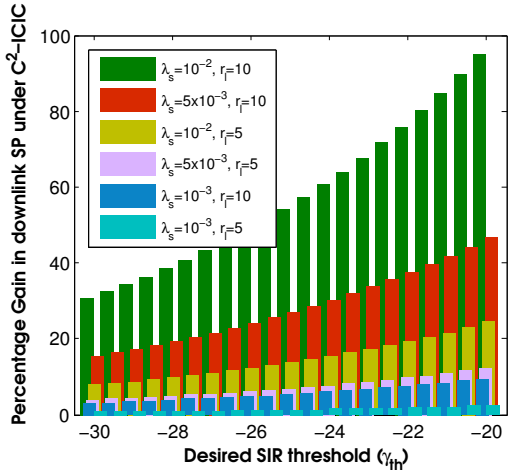

Figure 3: Percentage gain in downlink SP with and without C^2-ICIC with a varying desired SIR threshold (γ_{th}) when $\alpha = 4$ and $I_{th} = -5$ dBm (see (3) & (4)).

under the Rayleigh fading environment ($m_{\boldsymbol{ox}} = 1$). Moreover, the large-scale shadowing also reduces the downlink SP.

Fig. 3 plots the percentage gain obtained for the link level SP (and consequently the throughput) for the scheduled MU when using the C^2-ICIC scheme. The percentage gain can be quantified by employing Eq. (5) along with (3) and (4). We restrict our attention to the high SP regime. As shown in Fig. 3, a peak gain of around 100% can be experienced under the proposed coordination mechanism. It can be easily observed that as the density of the co-channel RRHs increases, the performance gain under coordination also increases for a certain fixed desired SIR (γ_{th}) and interference protection (I_{th}) thresholds. This can be attributed to the fact that in ultra dense networks, the proposed mechanisms can provide more effective interference control by restricting concurrent transmissions from the RRHs which violates the required protection constraint. Consequently, a significant gain is experienced in contrast to the non-coordinated transmission scheduling. Another important observation from Fig. 3 is that the gains experienced increase with an increase in the link distance between the MU and the serving RRH. In other words, MUs with lower received signal power can benefit more from the coordination as compared to the users whose signal strengths are relatively high. Intuitively, the SP performance of a weak MU is more susceptible to the variations in the aggregate interference than a user that lies near a small cell since the received signal strength decays with the distance following the power-law. Thus, a reduction in the co-channel interference provides significant gains for the weak users. As a matter of fact, following the LTE ICIC methods, the frame has to be divided into two distinct sub-frames. Out of these two distinct resource sub-frames, one should be employed to serve users without any coordination as long as the desired QoS is met. The second sub-frame could be employed to serve weak users under the proposed C^2-ICIC scheme. The optimal dimensioning of the sub-frame duration is an open issue which will be addressed in a future work.

D. Downlink Throughput

The downlink throughput of the scheduled MU is defined as the number of bits per second per Hertz that can be transmitted successfully over the link between the MU and its serving RRH. Mathematically,

$$\mathcal{T}^{i}_{\mathcal{MU}} = \log_2\left(1+\gamma_{th}\right) \times \mathbb{P}^{i}_{\mathcal{MU}}\left(\gamma_{th}, r_l\right) \text{ (bits/s/Hz)} \quad \text{where } i \in \{w, wo\}. \tag{10}$$

Fig. 4a displays the downlink throughput for a MU as a function of the desired SIR threshold, the density of co-channel active small cells and the link distance under Rayleigh fading environment. It can be observed that there exists an optimal SIR threshold which maximizes the link level throughput. It can be shown that in the absence of coordination, the optimal SIR threshold is only dependent upon the path-loss exponent and can

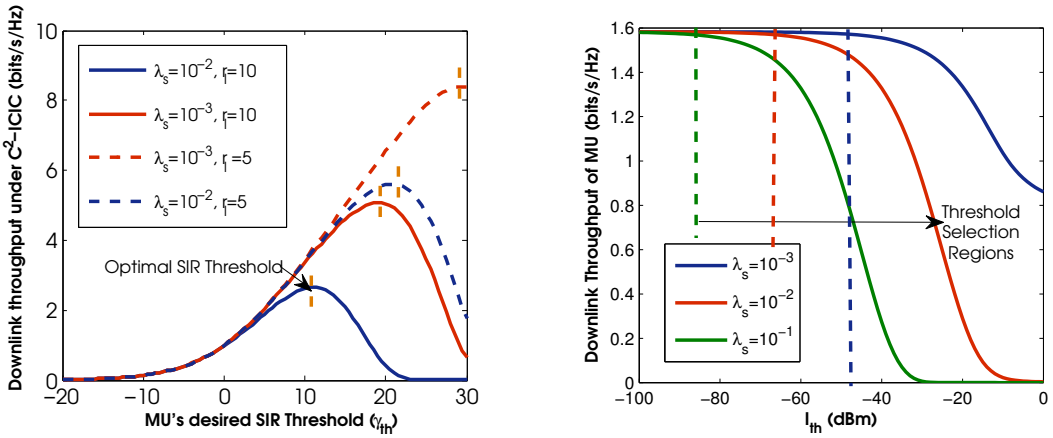

(a) Downlink throughput for a MU under the C^2-ICIC with a varying desired SIR threshold (γ_{th}) when $\alpha = 4$, $I_{th} = -50$ dBm and $P_s = 1$ (see Eq. (10)).

(b) Downlink throughput for a MU under the C^2-ICIC with a varying Interference threshold (I_{th}) when $\alpha = 4$, $\gamma_{th} = 0$ dBm and $P_s = 1$ (see Eq. (10)).

Figure 4: Downlink Throughput for a MU under C^2-ICIC Scheme.

be obtained as

$$\gamma^*_{th} = \exp\left(-\mathcal{W}\left(-\delta\exp(-\delta)\right) + \delta\right) - 1, \tag{11}$$

where $\mathcal{W}(.)$ is the principal branch of Lambert W function[4]. However, the optimal SIR threshold for the C^2-ICIC scheme is strongly coupled with both the co-channel small cell RRH density and the link distance. Deriving a closed-form expression for the optimal SIR is not tractable. Nevertheless, the optimal operating point can be numerically obtained by plotting Eq. (10) over a range of SIR values as in Fig. 4a. As demonstrated in Fig. 4a, the optimal SIR threshold increases with a decrease in either the RRH density or the link distance.

Design Consideration

From (1) it is obvious that the C^2-ICIC mechanism introduces a cap on the interference caused by each co-channel small cell. Nevertheless, bounding the interference inflicted by the individual RRHs does not translate into the aggregate interference control in a straightforward manner. The interaction between the local interference threshold (I_{th}) and the downlink SP due to the aggregate interference is given in (2) and (3). The coordinated small cells must adapt the local interference threshold (I_{th}) such that the downlink throughput of the scheduled MU can be maintained at a certain desired level. At the same time, I_{th} should be as large as possible to simultaneously schedule as many downlink transmissions as possible to maximize the network level throughput. Thus, the selection of I_{th} can be formulated as an optimization problem, which can be expressed as

$$I^*_{th} = \sup\left\{ I_{th} : \underbrace{\left(\lim_{I_{th}\to 0} \mathcal{T}^w_{\mathcal{MU}}(I_{th})\right)}_{\mathcal{T}_{max}} - \mathcal{T}^w_{\mathcal{MU}}(I_{th}) \approx 0 \right\}, \tag{12}$$

where $\mathcal{T}_{max}$ is the maximum attainable throughput. Notice that the optimization can be visualized with the help of Fig. 4b which shows that the downlink throughput for the MU saturates to $\mathcal{T}_{max}$ and further reduction of I_{th} does not bear any additional gain. While the throughput saturates to $\mathcal{T}_{max}$ irrespective of λ_S, the rate at which it saturates is a function of the small cell density. Thus for a particular fixed density, the threshold must be adapted according to Eq. (12).

Finally, we note that one of the limitations of the proposed framework is that it assumes that the fading severity parameter m assumes an integer value. This assumption is widely prevalent in the literature, mainly due to the analytical tractability. However, for non-integer values of m, upper and lower bounds can be obtained by performing ceil() and floor() operations on the fading severity parameter and then employing the proposed framework. Moreover, the optimization of I_{th} considering the network level throughput is also an open issue which is deferred to future work.

IV. Conclusion

In this article, we propose a cloud empowered cognitive inter-cell interference coordination (C^2-ICIC) scheme. The proposed scheme unifies the evolving phantom cell and cloud radio access network concepts. The proposed scheme is complemented by exploiting a channel state information aware threshold-based cognitive interference protection. Such a scheme restricts the interference from the individual co-channel small cell transmitters to remain below a prescribed threshold I_{th}. The aggregate interference experienced at the scheduled user is a function of the threshold constraint enforced at the individual small cells. Thus, the threshold must be selected judiciously to attain a certain desired downlink performance for the MU served under the coordination mode. Borrowing well established tools from stochastic geometry, we characterize the downlink success probability for a MU scheduled under the proposed C^2-ICIC scheme. We demonstrate that the proposed coordination strategy can provide percentage gains of the order of 100% for ultra dense small cell deployment. It is also shown that the C^2-ICIC scheme significantly improves the performance of the MUs experiencing low received signal strengths. The derived closed-form expression for the downlink success probability is employed to characterize the link level throughput for the MU. Since the selection of I_{th} controls spectrum access for the small cells operating in the coordination mode, its value should be as high as possible while ensuring near zero-deterioration to the scheduled MU. This manifests itself as a link level vs. network level throughput trade-off, which is briefly discussed in this article.

[4]The result follows from employing similar steps as in [16] Proposition 6.

References

[1] A. Ericsson, "Ericsson mobility report, february 2014," 2014.

[2] Ericsson, "Traffic and market data report: On the pulse of the networked society," *White Paper*, 2012.

[3] C. Mobile, "C-ran: the road towards green ran," *White Paper, ver*, vol. 2, 2011.

[4] H. Ishii, Y. Kishiyama, and H. Takahashi, "A novel architecture for lte-b: C-plane/u-plane split and phantom cell concept," in *IEEE Globecom Workshops (GC Wkshps)*. IEEE, 2012, pp. 624–630.

[5] K. Sung, M. Tercero, and J. Zander, "Aggregate interference in secondary access with interference protection," *IEEE Communications Letters*, vol. 15, no. 6, pp. 629–631, 2011.

[6] C. H. de Lima, M. Bennis, and M. Latva-aho, "Coordination mechanisms for self-organizing femtocells in two-tier coexistence scenarios," *IEEE Transactions on Wireless Communications*, vol. 11, no. 6, pp. 2212–2223, 2012.

[7] C. H. de Lima, M. Bennis, and M. Latva-Aho, "Statistical analysis of self-organizing networks with biased cell association and interference avoidance," *IEEE Transactions on Vehicular Technology*, vol. 62, no. 5, pp. 1950–1961, 2013.

[8] A. Ghasemi and E. Sousa, "Interference aggregation in spectrum-sensing cognitive wireless networks," *IEEE Journal of Selected Topics in Signal Processing*, vol. 2, no. 1, pp. 41–56, 2008.

[9] S. A. R. Zaidi, D. McLernon, and M. Ghogho, "Outage probability analysis of cognitive radio networks under self-coexistence constraint," in *44th Annual Conference on Information Sciences and Systems (CISS)*, 2010.

[10] A. Rabbachin, T. Quek, H. Shin, and M. Win, "Cognitive network interference," *IEEE Journal on Selected Areas in Communication*, vol. 29, no. 2, 2011.

[11] X. Hong, C. Wang, and J. Thompson, "Interference modeling of cognitive radio networks," in *IEEE Vehicular Technology Conference, VTC Spring*, 2008, pp. 1851–1855.

[12] M. Vu, S. Ghassemzadeh, and V. Tarokh, "Interference in a cognitive network with beacon," in *IEEE Wireless Communications and Networking Conference*, 2008, pp. 876–881.

[13] S.-H. Park, O. Simeone, O. Sahin, and S. Shamai, "Inter-cluster design of precoding and fronthaul compression for cloud radio access networks," *IEEE Wireless Communications Letters*, vol. 3, no. 4, pp. 369–372, Aug 2014.

[14] V. Nguyen and L. B. Le, "Joint coordinated beamforming and admission control for fronthaul constrained cloud-rans," *IEEE Globecom 2014*, 2014.

[15] D. Stoyan, W. Kendall, J. Mecke, and D. Kendall, *Stochastic Geometry and its Applications*. Wiley New York, 1995.

[16] M. Haenggi, "Outage, local throughput, and capacity of random wireless networks," *IEEE Transactions on Wireless Communications*, vol. 8, no. 8, pp. 4350–4359, 2009.

[17] S. A. R. Zaidi, M. Ghogho, D. C. McLernon, and A. Swami, "Achievable spatial throughput in multi-antenna cognitive underlay networks with multi-hop relaying." *IEEE Journal on Selected Areas in Communications*, vol. 31, no. 8, pp. 1543–1558, 2013.

[18] M. Haenggi and R. K. Ganti, *Interference in large wireless networks*. Now Publishers Inc, 2009, vol. 3, no. 2.

APPENDIX A
PROOF OF LEMMA 1

The proof follows standard steps, similar to Theorem 1 in [17]. However, for the sake of both completeness and to highlight the more general channel model considered here, we briefly sketch the proof as follows

$$\mathbb{P}_{\mathcal{MU}}\left(\gamma_{th}, r_l\right) = \Pr\left\{\frac{P_s h_{\boldsymbol{x}} l(r_l)}{P_s \sum_{\boldsymbol{y}\in\Pi} h_{\boldsymbol{y}} l(r_{\boldsymbol{y}})} > \gamma_{th}\right\},$$

$$= \mathbb{E}_I\left[\Pr\left\{h_{\boldsymbol{x}} > \gamma_{th} r_l^{\alpha} I\right\}\right] = \mathbb{E}_{I,g_{1p}}\left[\Pr\left\{g_{2\boldsymbol{x}} > \frac{\gamma_{th} r_l^{\alpha} I}{g_{1\boldsymbol{x}}}\right\}\right]$$

$$\overset{(a)}{=} \mathbb{E}_{\bar{I}}\left[\frac{\Gamma\left(m_{\boldsymbol{ox}}, m_{\boldsymbol{ox}}\gamma_{th} r_l^{\alpha}\bar{I}\right)}{\Gamma(m_{\boldsymbol{ox}})}\right] \overset{(b)}{=} \mathbb{E}_{\bar{I}}\left[\sum_{i=0}^{m_{\boldsymbol{ox}}-1}\frac{(s\bar{I})^i e^{-sI}}{i!}\right]$$

$$\overset{(c)}{=} \sum_{i=0}^{m_{\boldsymbol{ox}}-1}\frac{(-s)^i}{i!}\frac{\partial^i \mathcal{L}_I(s)}{\partial s^i}\bigg|_{s=\gamma_{th} r_l^{\alpha}}.$$

where (a) follows from the CDF of the Gamma random variable $g_{2\boldsymbol{x}}$; (b) follows from the identity $\Gamma(s,x) = (s-1)!\exp(-x)\sum_{i=0}^{s-1}\frac{x^i}{i!}$ for $s \in \mathbb{Z}^+$and (c) follows by changing the order of expectation and differentiation. Notice that for sake of simplicity, in (c) we slightly depart from the usual notation. More specifically, $\bar{I} = \sum_{\boldsymbol{y}\in\Pi}\frac{h_{\boldsymbol{y}} l(r_{\boldsymbol{y}})}{g_{1\boldsymbol{x}}}$ is denoted by I, this is because $\frac{h_{\boldsymbol{y}}}{g_{1\boldsymbol{x}}} = \frac{g_{1\boldsymbol{y}} g_{2\boldsymbol{y}}}{g_{1\boldsymbol{x}}}$ can be written as $h_{\boldsymbol{y}} = \bar{g}_{1\boldsymbol{y}} g_{2\boldsymbol{y}}$ where $\bar{g_{1\boldsymbol{y}}} = \exp\left(\zeta\left(\sigma_{\boldsymbol{ox}} + \sigma_{\boldsymbol{oy}}\right)Z\right)$ is a Log-normal random variable. This follows from the fact that the ratio of two Log-normal random variable follows the same law.

APPENDIX B
PROOF OF THEOREM 1

In the absence of C^2-ICIC, the aggregate interference can be characterized by using the fact that

$$\begin{aligned}\mathcal{L}_I(s) &= \mathbb{E}_{r,H}\left[\exp\left(-\sum_{\boldsymbol{y}\in\Pi_{\mathcal{S}}^{TX}} h_{\boldsymbol{y}} l(r_{\boldsymbol{y}})\right)\right], \qquad (13)\\ &\overset{(a)}{=} \exp\left(\int_{\mathbb{R}}\left(1-\mathbb{E}_h\left\{\exp\left(-hr^{-\alpha}\right)\right\}\right)\lambda_{\mathcal{S}} 2\pi r dr\right),\\ &\overset{(b)}{=} \exp\left(-\lambda_{\mathcal{S}}\pi\mathbb{E}_h(h^{\delta})\Gamma\left(1-\delta\right)s^{\delta}\right),\end{aligned}$$

where (a) follows from the definition of the Generating functional for the HPPP [15] and (b) follows from evaluating the integral as in Eq. (3.20) of [18]. The proof can be concluded by evaluating the δ^{th} moment of $g_{2\boldsymbol{y}}$ which is Gamma distributed, i.e., $\mathbb{E}\left(g_{2\boldsymbol{y}}\right) = \frac{\Gamma(m_{\boldsymbol{oy}}+\delta)}{\Gamma(m_{\boldsymbol{oy}})m_{\boldsymbol{oy}}^{\delta}}$ and $\mathbb{E}\left(g_{1\boldsymbol{y}}\right) = \exp\left(\frac{1}{2}\left(\frac{(\sigma_{\boldsymbol{xo}}+\sigma_{\boldsymbol{yo}})\zeta}{\alpha}\right)^2\right)$ and employing Lemma 1.

APPENDIX C
PROOF OF THEOREM 2

The integral in A_1 can be evaluated by letting $w(r,h) = 1-\exp\left(-shr^{-\alpha}\right)$ then

$$\begin{aligned}A_1 &= \mathbb{E}_h\left(\int_0^{\infty} w(r,h)\lambda_{\mathcal{S}} 2\pi r \mathbb{1}_{I_{th}}(r,h)\,dr\right),\\ &= \mathbb{E}_h\left(\int_0^{\infty} w(r,h)\lambda_{\mathcal{S}} 2\pi r \mathbb{1}_{I_{th}}\left(P_s h r^{-\alpha} \le I_{th}\right)dr\right),\\ &= \mathbb{E}_h\left(\int_0^{\infty} w(r,h)\lambda_{\mathcal{S}} 2\pi r \mathbb{1}_{I_{th}}\left(r \ge \left(h/\bar{I}_{th}\right)^{1/\alpha}\right)dr\right),\\ &= \mathbb{E}_h\left(\underbrace{\int_{\left(h/\bar{I}_{th}\right)^{1/\alpha}}^{\infty} w(r,h)\lambda_{\mathcal{S}} 2\pi r\,dr}_{B_1}\right), \qquad (14)\end{aligned}$$

Let $z = \left(h/\bar{I}_{th}\right)^{1/\alpha}$ and $\delta = \frac{2}{\alpha}$, then B_1 can be evaluated by using integration by parts as

$$\begin{aligned}B_1 &= \lambda_{\mathcal{S}}\pi\left[\left(1-\exp\left(-shr^{-\alpha}\right)\right)r^2\Big|_z^{\infty}\right.\\ &+ \left.\alpha\int_z^{\infty} shr^{1-\alpha}\exp(-shr^{-\alpha})dr\right]\\ &= \lambda_{\mathcal{S}}\pi\left[h^{\delta}s^{\delta}\gamma_l\left(1-\delta, s\bar{I}_{th}\right) - \bar{I}_{th}^{-\delta}h^{\delta}\right.\\ &\times \left.\left(1-\exp\left(-s\bar{I}_{th}\right)\right)\right].\end{aligned}$$